Article

Not peer-reviewed version

Testing and Characterizing Commercial 18650 Lithium-Ion Batteries

Nicolò Zatta , Bernardo De Cesaro , Enrico Dal Cin , Gianluca Carraro , Giovanni Cristofoli , Andrea Trovò , Andrea Lazzaretto , Massimo Guarnieri *

Posted Date: 21 May 2024

doi: 10.20944/preprints202405.1399.v1

Keywords: Li-ion cell; cylindrical cell; 18650 cell; cell parameter identification; cell equivalent circuit model; galvanostatic intermittent tritation technique; cell entropic heat; coupled electro-thermal model

 doi:10.20944/preprints202405.1399.v1

Article

Testing and Characterizing Commercial 18650 Lithium-Ion Batteries

Nicolò Zatta [1,2], Bernardo De Cesaro [1], Enrico Dal Cin [1], Gianluca Carraro [1], Giovanni Cristofoli [3], Andrea Trovò [1,2], Andrea Lazzaretto [1] and Massimo Guarnieri [1,2]*

[1] Department of Industrial Engineering, University of Padua, 35131 Padova, Italy; nicolo.zatta@phd.unipd.it (N.Z.); bernardo.decesaro@studenti.unipd.it (B.D.C.); enrico.dalcin@phd.unipd.it (E.D.C.); gianluca.carro@unipd.it (G.C.); andrea.trovo@unipd.it (A.T.); andrea.lazzaretto@unipd.it (A.L.); massimo.guarnieri@unipd.it (M.G.)

[2] Interdepartmental Centre Giorgio Levi Cases for Energy Economics and Technology, University of Padua, 35131 Padova, Italy

[3] FIAMM Energy Technology S.p.A., Montecchio Maggiore 36075, Italy; GC2: giovanni.cristofoli@fiamm.com

* Correspondence: massimo.guarnieri@unipd.it Tel.:+390498277524

Abstract: Reduced-order electrothermal models play a key role in the design and control of lithium-ion cell stacks, calling for accurate model parameter calibration. This paper presents a complete electrical and thermal experimental characterization procedure for coupled modeling of cylindrical lithium-ion cells in order to implement them in a prototype Formula SAE hybrid racing car. The main goal of the tests is to determine cell capacity variations with temperatures and discharge currents, to predict the open circuit voltage of the cell and its entropic component. A simple approach for the characterization of the battery equivalent electrical circuit and a two-steps thermal characterization method are also shown. The investigations are carried out on four commercial 18650 NMC lithium cells. The model demonstrated to predict the battery voltage at a RMS error lower than 20 mV and the temperature to a RMS error equal to 0.5 °C. The authors hope that this manuscript can contribute to the development of standardized characterization techniques for such cells, while offering experimental data and validated models that can be used by researchers and BMS designers in different applications.

Keywords: Li-ion cell; cylindrical cell; 18650 cell; cell parameter identification; cell equivalent circuit model; galvanostatic intermittent tritation technique; cell entropic heat; coupled electro-thermal model

1. Introduction

Thanks to the high energy density and specific energy [1], lithium-ion batteries have gone through a dizzying diffusion in recent years, both in the automotive sector (passing from a market share of 0.2 in 2013 to 13% in 2022 [2]) and for portable electronic devices (15 billion of mobile phones in the world in 2021 [3]). Cells are typically assembled in modules, or packs, to achieve the desired battery rating. In modules, cells are connected both in series and in parallel to attain the desired voltage and energy capacity. For instance, many electric cars operate in the range 400-800 volts, while individual cells generally have voltages ranging from 3-4 volts. The proper and safe module operation is ensured by the Battery Management System (BMS), whose effective design calls for an accurate and physically consistent electrical and thermal model of the Li-ion pack [4]. This applies to several BMS features, such as: State of Charge (*SoC*) measurements, State of Health (*SoH*) estimation (also in extreme conditions), circuit balancing and thermal runaway detection and suppression to preclude fire hazards.

As regards the last issue, the acceptable operational temperature for Li-ion cells spans from -20 to 60 °C, with optimal performance occurring between 15 °C and 35 °C. Nevertheless, heat generation within a Li-ion battery pack is inevitable due to various losses and entropic effects, resulting in a uneven temperature distribution with gradients among module cells. Uncontrolled heat generation can lead not

 doi:10.20944/preprints202405.1399.v1

only to thermal runaway but also to capacity loss and cell instability, so that the temperature differences among cells should be limited to 6 °C to ensure optimal operation and preserve the battery *SoH*.

Developing a BMS is a complex task that entails creating reduced battery models, estimators, and functionalities to guarantee the battery optimal performance in all operating conditions and throughout its entire lifespan. All of them must operate with limited computational resources on a cost-effective microcontroller. This calls for significant expertise and technical know-how, which may lack in a framework of a rapidly developing technology, a condition particularly evident in the battery industry with emerging chemistries, each presenting its own challenges, requirement and features. To address this, an accurate characterization of the cells is vital.

This paper describes some electrical and thermal experimental characterization procedures conceived for producing with high accuracy all the cell physical parameters needed in a reliable electrical and thermal lumped models. Four commercial 18650 Li-ion cells of different manufacturers have been considered: Molicel® P28A, P28B and P30B and Sony Murata VTC5D. The following parameters have been obtained: the cell capacity at different temperatures and discharge currents (C-rates), the Open Circuit Voltage (OCV) at varying State of Charge (*SoC*), the entropic coefficient and electrical and thermal lumped parameters.

This work is part of a collaborative research between three groups within the Department of Industrial Engineering (DII) of the University of Padua (Padova, Italy): Electrochemical Energy Storage and Conversion Lab (EESCOLab), Modelling, Analysis and Research in Turbomachinery and Energy Systems (MARTES), RaceUp Formula SAE Students Team, togheter with the company FIAMM Energy Technology S.p.A. The target of this work is to analyse different lithium-ion cells in order to implement them in a prototype Formula SAE hybrid racing car. Formula SAE is a student design competition program organized by SAE International (previously known as the Society of Automotive Engineers). Few articles in the literature report accurate descriptions of measurement techniques, experimental results and their use in suitably validated models. For the sake of comparison, different techniques published in the literature are also detailed. The obtained models demonstrated to successfully predict the battery voltage at a 8 RMS error lower than 20 mV and the temperature to a RMS error equal to 0.5 °C. The authors hope that this this manuscript can be useful for the development of standardized characterization techniques of such cells, while also providing experimental data and validated models that researchers and BMS designers can utilize across various applications.

Section 2 describes the reduced-order modeling of 18650 cells, both thermal and electrical. Section 3 describes the methods for the electrical and thermal characterization of the four type of cells. The former concern the determination of the cell capacity at different C-rate currents and temperatures, the dependence of the OCV with the *SoC*, the impulsive current charge/discharge tests to identified the Equivalent Circuit Model (ECM) parameters and the determination of the entropic contribution. The thermal characterization deals with the methods for determining the main thermal parameters involved in thermal modeling, i.e. the cell thermal capacity, the conduction thermal resistance between cell bulk and surface and the convection thermal resistance between the cell surface and environment. In Section 4 the validation of the battery models for four different load profiles is presented, demonstrating their good accuracy. The significance of this work is finally outlined in the conclusion in Section 5.

2. Reduced-Order Coupled Modeling of 18650 Cells

Several approaches are presented in the literature to develop reduced-order models capable of predicting the battery voltage and temperature for short dynamic current cycle [5,6], spanning from electrochemical-based to circuit-based types, as well as empirical and data-driven models for voltage prediction coupled with thermal models. Due to ease of characterization and implementation in Simulink [7], an Electrical Circuit Model (ECM) approach was chosen to model the cell electrical behaviour, coupled with an array-based thermal circuit model simulating the battery temperatures.

 doi:10.20944/preprints202405.1399.v1

The ECM, represented in Figure 1, consists of a voltage source U_{OC} giving the cell OCV, a resistor R_s and the series of two RC loops, each consisting of a resistor R_i and a capacitor C_i. Similar models using only resistors and capacitors as passive elements are largely presented in the literature ([8–10]). To account for the effects of the physical conditions on the cell performance, the ECM elements were assumed to be driven as follows: U_{oc} is driven by the SoC, while R_s, R_i and C_i are driven by the SoC, operating temperature and current sign. Consistently with the targeted model accuracy, minor dependencies such as current magnitude and aging, were neglected [10,11].

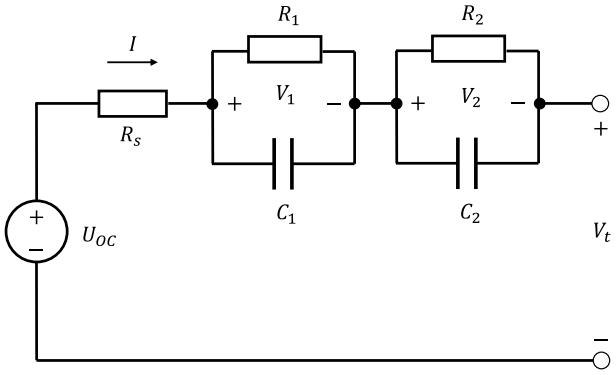

Figure 1. Equivalent circuit model diagram for a cylindrical Li-ion cell.

The electrical model is coupled with the thermal model through the heat generation equation [12]:

$$Q = I(V_t - U_{OC}) + IT_{avg}\frac{dU}{dT} \tag{1}$$

where T_{avg} [K] is the battery average temperature and dU/dT [V K^{-1}] is the entropic coefficient, i.e. the temperature derivative of the OCV, that depends on the SoC [13].

The lumped thermal model is shown in Figure 2. As commonly done in literature [12,14], the battery surface temperature was assumed homogeneous and the battery thermal behaviour perfectly axis-symmetric, so that heat exchanges at the top and bottom cell caps were neglected. The room temperature was assumed homogeneous and constant. The battery casing thermal capacity was neglected, because it was considered orders of magnitude smaller than the cell one [15].

The equations of the thermal model are reported in Equation 2:

$$\begin{cases} C_c\dfrac{dT_c}{dt} = \dfrac{T_s - T_c}{R_c} + Q \\ 0 = \dfrac{T_{air} - T_s}{R_u} + \dfrac{T_c - T_s}{R_c} \end{cases} \tag{2}$$

where T_c is the cell bulk temperature, T_s is the cell surface temperature, C_c is the cell thermal capacity, R_c is the conduction thermal resistance between cell bulk and surface and R_u is the convection thermal resistance between the cell surface and the room, while Q is the heat rate, generated by the cell losses.

Preprints.org (www.preprints.org) | NOT PEER-REVIEWED | Posted: 21 May 2024 doi:10.20944/preprints202405.1399.v1

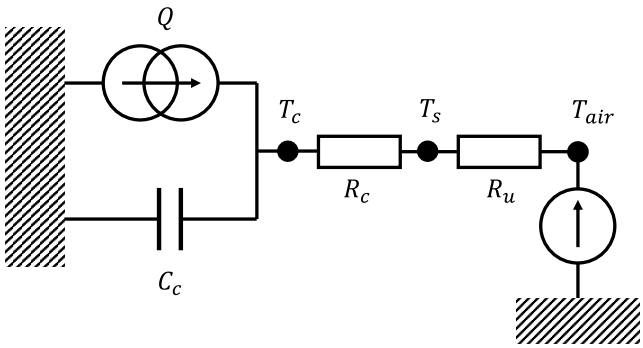

Figure 2. Thermal array scheme for a cylindrical Li-ion cell.

3. Testing and Characterization

3.1. Materials and Experimental Set-Up

Four commericial 18650 Li-ion cells of different manufacturers underwent the testing procedure: Molicel® P28A, P28B and P30B and Sony Murata VTC5D (Figure 3.) In Table 1, the cells characteristics and performance are reported as from the manufacturers data-sheet.

Figure 3. The four cells tested: from left to right, Molicel P28A, P28B, P30B, and Sony Murata VTC5D.

Table 1. Parameters for the tested cells (Manufacturers data-sheets).

	P28A	**P28B**	**P30B**	**VTC5D**
Nominal capacity [mAh]	2800	2800	3000	2800
Minimum capacity [mAh]	2600	2650	2900	2500
Upper cut-off voltage [V]		4.2		
Lower cut-off voltage [V]		2.5		
Max. continuous discharge current [A]	35	40	30	30
Discharge temperature range [C°]	−40/+60	−40/+60	−40/+60	−20/+60
Internal resistance [mΩ]	20	21	17	n.r.
Size [mm]		⌀≈ 18.6, h ≈ 65.2		
Mass [g]	46	48	47	44

The tests were mostly conducted in the laboratories of FIAMM Energy Technology using the following major equipment:

- Thermal chamber Binder Mk115, to maintain constant operating temperature in each experiment and to allow testing at different temperatures.
- Four-terminal sensing cell holder: a BioLogic CBH-4 was used for electrical tests,.

 doi:10.20944/preprints202405.1399.v1

- In-house polymeric cell holder for thermal tests.
- Thermocouples array, to detect the battery surface temperature and the room temperature in side the thermal chamber, connected to a Hioki LR8450 data logger.
- Cell cycler, consisting of a Rohde&Schwarz® HMP4040 charger and a) a Rigol DLC3031 load, to measure the entropic contribution and the pseudo-U_{OC} experiment, and b) a Digatron Systems UBT150-020 for other tests.

The experimental set-up was controlled by a PC and data were post-processed in MatLab and Simulink environments. Figure 4 shows a scheme of the experimental set-up.

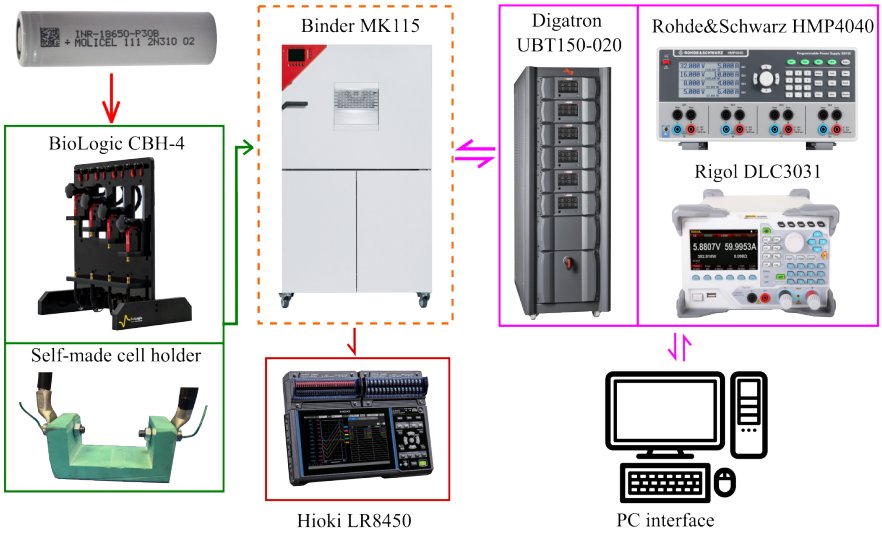

Figure 4. The experimental set-up used at FIAMM lab consisting of (left to right): two cell holders, a thermal chamber, two cell cycler sets, a thermocouple array with data logger, a control and data processing pc.

3.2. Electrical Characterization Tests

3.2.1. Capacity Determination

The battery capacity at the Beginning of Life (BoL) is an important Key Performance Indicator (KPI) for applications where the long cycle life is not a driving design parameters, as in the case of the target application of this work, i.e. a FSAE racing car [16–18].

In order to evaluate the dependence of cell capacity on the temperature and discharge current, as in [19–22], the following testing procedure was implemented:

1. Fully charge the cell to $SoC = 100\%$ with a) 1 C Constant Current (CC) till the voltage reaches the upper cut-off (4.2 V) and b) Constant Voltage (CV) till the current reduces to the rate C/20, at reference temperature $T_{ref} = 25\,^{\circ}\text{C}$.
2. Put the thermal chamber at the temperature T_i and wait 1 h to allow cell temperature and voltage relaxation.
3. Discharge the cell at CC with a rate $C_{r,i}$ till the voltage reduces to the lower cut-off voltage 2.5 V.
4. Bring the thermal chamber to the reference temperature T_{ref} and wait 1 h to allow cell temperature and voltage relaxation.
5. Repeat step 1-4 five times.

The testing procedure was run at $T_i = 5\,^{\circ}\text{C}$, $25\,^{\circ}\text{C}$, and $40\,^{\circ}\text{C}$ and at discharge currents with C-rate $C_{r,i} = 0.5\,\text{C}$, 1 C, 3 C, and 5 C. The cell charge capacity [mAh] for each test was computed as the time integral of the current during the CC discharge. To quantify the spread of performance among different cells of the same type [23], three samples for each model were tested and each of them underwent

 doi:10.20944/preprints202405.1399.v1

five discharges. The capacity of the cell model was then obtained as the average of such 15 tests. In addition, the standard deviations of these tests are are shown in Table 2.

Table 2. Capacity of the tested cells at different C-rate discharge currents and temperatures. Shown values are the averages and deviation among three cells per type and five discharges per each cell

	Temperature	0.5C	1C	3C	5C
	[°C]	[mAh]	[mAh]	[mAh]	[mAh]
P28A	5	2656 ± 20	2575 ± 10	2541 ± 10	2562 ± 10
	25	2747 ± 60	2685 ± 70	2620 ± 70	2606 ± 70
	40	2687 ± 30	2658 ± 20	2575 ± 20	2561 ± 30
P28B	5	2527 ± 30	2490 ± 20	2459 ± 10	2477 ± 20
	25	2720 ± 100	2670 ± 100	2581 ± 60	2567 ± 60
	40	2542 ± 30	2547 ± 20	2499 ± 30	2504 ± 80
P30B	5	2825 ± 60	2747 ± 40	2710 ± 30	2810 ± 20
	25	3041 ± 30	2943 ± 10	2915 ± 20	2908 ± 30
	40	3015 ± 40	2961 ± 20	2890 ± 10	2893 ± 10
VTC5D	5	2712 ± 50	2616 ± 20	2568 ± 50	2578 ± 50
	25	2861 ± 20	2791 ± 5	2685 ± 20	2668 ± 10
	40	2749 ± 50	2704 ± 40	2618 ± 60	2607 ± 40

3.2.2. OCV Measurements

Determining the dependence of U_{oc} on SoC is crucial to accurately predict the battery voltage V_t. The main experimental techniques for a priori OCV vs SoC measurements are the "pseudo-U_{oc} test", also referred to as "low current continuous OCV measurement", and the "intermittent current pulse test" [24,25]. Measurement data can be collected in look-up table or used to fit mathematical functions [26]. In the present work, the OCV vs SoC curve was obtained applying the pseudo-U_{oc} test for all the cells, conisting in the following procedure:

1. Fully charge the cell to $SoC = 100\%$ with a) 1 C Constant Current (CC) till the voltage reaches the upper cut-off (4.2 V) and b) a Constant Voltage (CV) till the current reduce to a rate C/20, at reference temperature $T_{ref} = 25\,°C$.
2. Relax the cell voltage for 1 h.
3. Discharge the cell with CC at a rate C/20 till the voltage reduces to the lower cut-off 2.5 V.
4. Charge the cell with CC at a rate C/20 till the voltage reaches the upper cut-off 4.2 V.

The cell OCV curve was obtained as the average between voltages in charge and discharge (Figure 5).

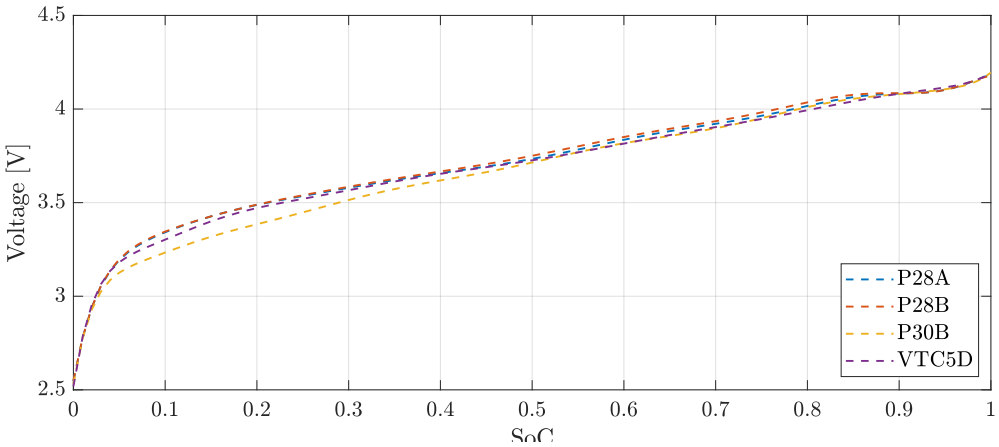

Figure 5. OCV vs SoC curves of the tested cells, obtained as averages in charge and discharge tests performed at C/20 current.

 doi:10.20944/preprints202405.1399.v1

This is a simple and reliable method, which has proven to be successful in the present application. Future developments may involve the use of more complex post-processing data algorithms, aimed at identifying voltage hysteresis in OCV measurements [27], correcting partial relaxations effects during pulse tests [28], or implementing filtering techniques (*e.g.*, Kalman filters) as in [29].

3.2.3. GITT characterization tests

Impulsive current charge/discharge tests are commonly presented in literature to determine the ECM parameters of lithium-ion batteries [10,12,30]. Such impulsive test take different names, e.g. Galvanostatic Intermittent Titration Technique (GITT) test. Considering the ECM decribed above, the test was oriented to identify the circuit parameters in charge and discharge at different operating temperatures. The testing procedure used for GITT characterization was as follows:

1. Fully charge the cell ($SoC = 100\%$) with a) 1 C Constant Current (CC) till the voltage reacheas the upper cut-off (4.2 V) and b) Constant Voltage (CV) till the current reduced to a rate C/20, at reference temperature T_{ref} = 25 °C.
2. Relaxe the cell voltage for 1 h.
3. Impose a discharge 2 C current impulse lasting for τ_{imp}, then relax the battery voltage for 1 h.
4. Repeat 3 till the voltage reachers the lower cut-off 2.5 V, then relax the battery voltage for 1 h.
5. Repeat 3 with charge current impulse till the voltages reachers the upper cut-off 4.2 V.
6. Repeat the impulsive test at 5 and 40 °C.

The duration of the load impulse τ_{imp} varied between 180 s when $25\% \leq SoC \leq 75\%$, and 72 s otherwise.

Data-post processing consisted in an optimization procedure, with the goal of minimizing the error between the cell voltage measured during experiments and that computed with ECM-based simulations. The output of the GITT characterization was a set of look-up tables defined for different temperatures and SoCs, in charge and discharge. The optimization problem was developed in the Matlab Optimization Toolbox making use of the `lsqnonlin` solver. A finite difference approximation approach was used to implement ECM behaviour. The differentiation time step corresponded to the sampling frequency of cell voltage during experiments. To reduce the computational cost, instead of performing a single optimization through the entire GITT test, independent optimizations were run for each GITT cycle (pulse and relaxation), corresponding to given *SoC*, temperature, and current sign. The output parameters calculated for a given cycle were then used as guess values for the subsequent one, which resulted in a layered approach [8]. Figure 6 shows the experimental and modelled GITT test voltages , while the ECM parameters tables for the four tested cell models are reported in Appendix.

 doi:10.20944/preprints202405.1399.v1

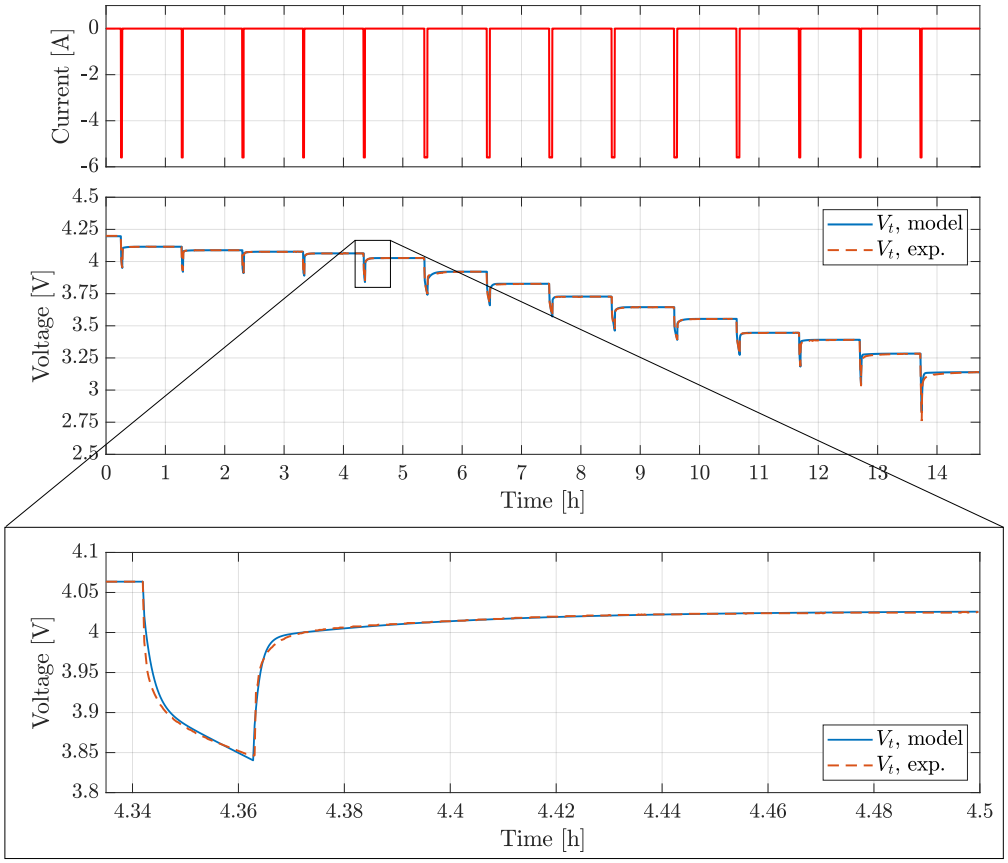

Figure 6. Experimental and fitted fata for of the discharge GITT test for the P28B cell at 25 °C.

3.3. Entropic Contribution Measurement

Entropic contribution of lithium-ion cells is traditionally determined from potentiometric and calorimetric measurements [31]. The former consists in measuring the cell OCV at different temperatures and *SoC*s [32]. A thermal cycle needs to be applied after complete relaxation of the cell voltage. In addition, at each temperature of the cycle the thermal equilibrium condition requires some time to be reached and the larger the thermal capacity of the cell, the larger the system thermal time constant [33]. Instead, the calorimetric method is based on the cell heat flux measurement during charge/discharge operations: the entropic contribution is determined after separating the irreversible and the reversible heat contributions in the overall measured heat flux [33]. This method can be considered superior to the potentiometric one, allowing for a quasi-continuous measurement of the cell entropic profile. On the other hand, it presents some disadvantages: many cell electrical parameters [34,35] have to be previously determined and advanced cell-specific experimental equipment is needed, as an isothermal or accelerating-rate calorimeters.

To overcome the limitations of the potentiometric and calorimetric methods, a novel $\partial U/\partial T$ determination technique via Electrothermal Impedance Spectroscopy (ETIS) has been developed by Schmidt *et al.* in [36]: a thermal transfer function is obtained to relate the surface temperature to the heat flux, then the reversible heat flux is split from the irreversible term by Fourier analysis. Such technique, used also by Geng *et al.* in [33], presents some drawbacks regarding the precise determination of a thermal transfer function and the spectroscopy data analysis [31].

Recently, different improved approaches have been proposed to reduce the testing time required by the potentiometric method, mainly in the form of correction of the voltage baseline drift, as in [37] and [31]. Furthermore, in [38] Lin *et al.* proposed an improved potentiometric method based on current Positive Adjustment Method (PAM). In the present work, the Common Potentiometric Method (CPM)

 doi:10.20944/preprints202405.1399.v1

was modified to reach the desired SoC, i.e. after a long charge (or discharge) phase an opposite current was applied for a short time. Such PAM was expected to accelerate the depolarization and reduce the voltage relaxation time (from 10 - 20 h of the CPM to ∼10 min of the PAM). The approach was validated by comparing the measured entropy profile of 18650 lithium ion cylindrical cells with those obtained from CPM: results showed good agreement between the two, thus confirming the advantage of saving test time.

A similar approach to the PAM was used in this paper. Considering that all cells are based on similar NMC chemistry and have similar forms, sizes and capacities, only the P30B model was tested. The testing procedure consisted of:

1. Fully charge the cell to $SoC = 100\%$ at the reference temperature $T_{ref} = 25\,°C$.
2. Relax the cell voltage for 20 h.
3. Apply a controlled thermal cycle (1 h at 20 °C, 1 h at 10 °C, 1 h at 30 °C, 1 h at 40 °C, 1 h at 25 °C).
4. Discharge the cell for τ_{entr} at 1 C rate and then charge at 0.1 C rate for $2 \times \tau_{entr}$.
5. Relax the cell voltage for 1 h.
6. Repeat step 3-5 till the voltage reaches the lower cut-off 2.5 V.

The value of τ_{entr} varied in order to collect more data points at high and at low SoC. Figure 7 shows the current profile imposed and the voltage measured at the cell terminals, with a zoom on the temperature profile for $U_{OC} = 3.832\,V$.

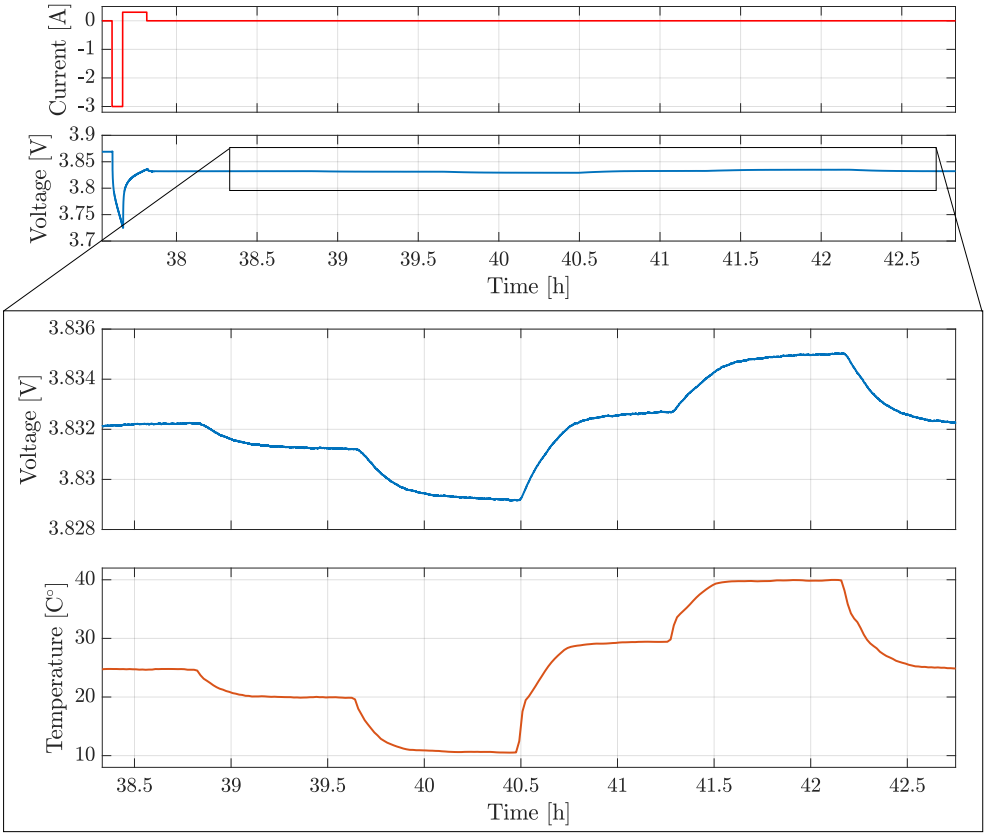

Figure 7. Positive Adjustment Method (PAM) applied on P30B cell, in order to measure the profile of the entropic contribution $\partial U/\partial T$: a step shaped current load is applied to the cell to reach the desired SoC measurement point. Then, after a relaxation time, a thermal cycle is applied.

During the PAM test, the battery Open Circuit Voltage (OCV) was measured at various temperatures and SoCs (Figure 8).

 doi:10.20944/preprints202405.1399.v1

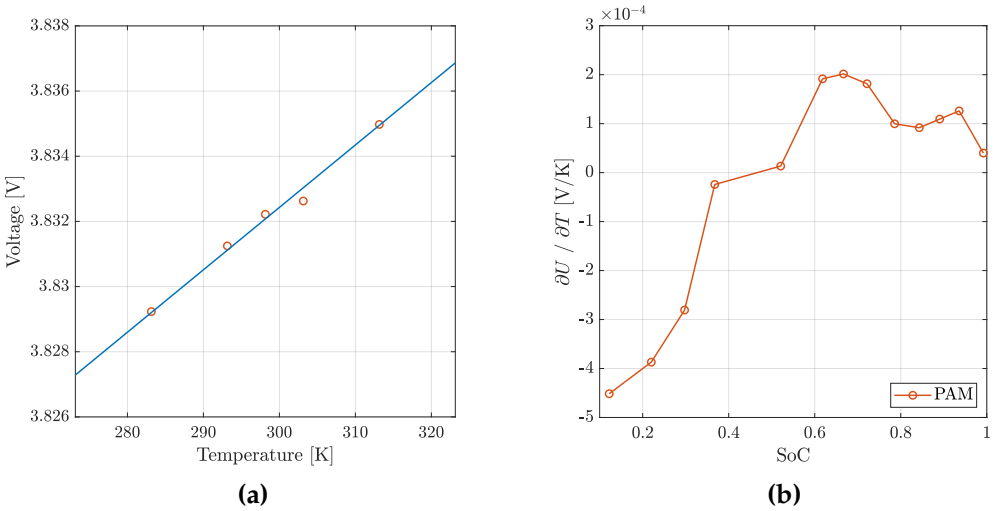

Figure 8. Measured OCV at various temperature and $SoC \approx 0.6$: for each SoC, the slope of the interpolation line is the $\partial U/\partial T$ term (**a**); the $\partial U/\partial T$ vs SoC for the P30B cell is reported in (**b**), showing good agreement with previous data from literature [38,39] .

3.4. Thermal Characterization Tests

The thermal parameters involved in thermal modeling of lithium ion cell can be identified in different ways. A common approach is to used calorimetric measurements to determine the battery heat capacity and the anisotropic thermal conductivity: Vertiz *et al.* [40] used Accelerating Rate Calorimeter (ARC) technique to determine heat capacity and thermal conductivity of a lithium-ion pouch cell, coupling an electrical circuit model to a thermal circuit model. Sheng *et al.* [41] imposed controlled heat flux to investigate thermal parameters of a prismatic lithium-ion cell, whereas Cao *et al.* studied the heat generation characteristics through heat flux measurements of commercial 18650 cells [42]. Calorimetric measurements, though precise, require expensive equipment: this is one of the reason why many papers on thermal modelling of Li-ion cells cited above adopted the volume-fraction method to determine the battery thermal parameters from the materials properties. This is the case of [43,44] or [45], where cylindrical cells are studied coupling a electrochemical model with a 2-D thermal model.

Other works present thermal characterization procedures based on cell surface temperature measurements and obtain the internal thermal parameters through numerical optimization studies. Al-Zareer *et al.* [46] determined the heat capacity and the radial and axial cell thermal conductivities by measuring the cell surface temperature and implementing an optimization routine on a COMSOL Multiphysics® 3-D model for a cylindrical 18650 cell. A similar approach to identify the heat transfer coefficient and the thermal parameters for a prismatic lithium-ion cell was adopted by Samad *et al.* [47] using MATLAB software and considering an array of surface temperature probes, coupling the thermal model with a two RC-loops ECM. Different online parameterization algorithms have also been proposed, in particular for BMS application for battery stacks, as that described by Lin *et al.* [48], which implemented a simple equivalent circuit-based thermal model, or that described in [49].

Bryden *et al.* [50] proposed a new method based on a non-invasive cell surface temperature measurements in two experimental heat transfer conditions: natural convection and forced convection. Such method, used also by Akbarzadeh *et al.* [9] on prismatic cells, allows a fast and easy thermal characterization and it is particularly suitable for equivalent thermal circuit models and for these reasons it was chosen in this work.

The experimental procedure applied to the cell model consisted of:

1. Fully charge the cell and then discharge to $SoC \approx 50\%$ at reference temperature $T_{ref} = 25\,^{\circ}\mathrm{C}$.
2. Relax the cell voltage and temperature for 1 h.

 doi:10.20944/preprints202405.1399.v1

3. Apply a square alternating wave load current with period of 120 s, a peak-to-peak amplitude corresponding to a rate of 6 C till reaching a steady-state thermal equilibrium on the cell surface. In this way, the entropic heat contribution could be neglected (see Equation 1).
4. Repeat step 1-3 in two heat exchange condition:

   *Cond*1) low-convective heat transfer condition (the cell is placed in the *CellHold*1 and exchanges heat by natural convection with the air inside the thermal chamber),

   *Cond*2) high-convective heat transfer condition (the cell is placed in *CellHold*1 and a pair of fans cools it down, so that heat exchange is mainly driven by forced convection).

In Equation 2, T_c in the first equation can be replaced giving:

$$C_c \left(1 + \frac{R_c}{R_u}\right) \frac{dT_s}{dt} = \frac{T_{air} - T_s}{R_u} + Q \tag{3}$$

By measuring V_t the time dependent heat rate Q was calculated: once reached the thermal quasi-stationary equilibrium condition ($T_{s,\text{inf}}$), we can estimate a first-try value for $R_{u,0}$ as:

$$R_{u,0} = \frac{T_{s,\infty} - T_{air}}{Q} \tag{4}$$

Considering the two different heat transfer conditions *Cond*1 and *Cond*2 and defining:

$$C_p^{'} = C_c \left(\frac{R_c}{R_u} + 1\right) \tag{5}$$

we can write Equation 3 as:

$$\begin{cases} C_{p,1}^{'} = C_c \left(\frac{R_c}{R_{u,1}} + 1\right) \\ C_{p,2}^{'} = C_c \left(\frac{R_c}{R_{u,2}} + 1\right) \end{cases} \tag{6}$$

A Levenberg-Marquardt optimization algorithm was run using the MATLAB routine `lsqcurvefit`: the value of $R_{u,1}$ and $R_{u,2}$ obtained from Equation 4 were considered as first tries, and the final values of $C_{p,1}^{'}$, $R_{u,1}$ and $C_{p,2}^{'}$, $R_{u,2}$ were calculated by minimizing the residuals between the modelled and the experimental temperature T_s in the two conditions. Eventually, the algebraic solution of Equation 6 system yielded C_c and R_c. Figure 9 shows the thermal characterization *Cond*1 and *Cond*2 test profiles of the P28A cell, revealing a good agreement between the experimental and simulated T_s profiles, obtained using the optimized thermal parameters.

The thermal model parameters obtained from the thermal characterization tests for four tested cell are listed in Table 3.

Preprints.org (www.preprints.org) | NOT PEER-REVIEWED | Posted: 21 May 2024 doi:10.20944/preprints202405.1399.v1

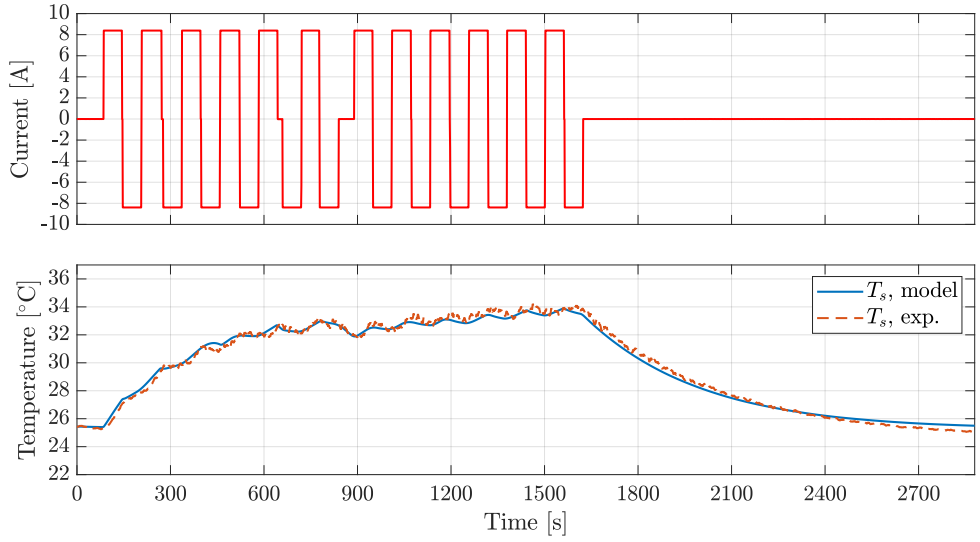

(a)

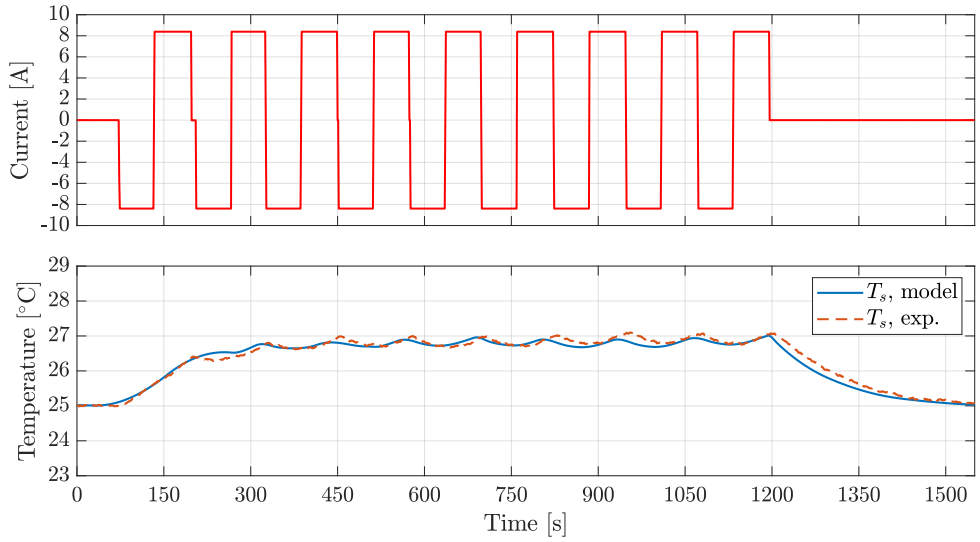

(b)

Figure 9. P28A cell thermal characterization tests: (**a**) low convective testing condition; (**b**) high convective testing condition. The experimental and the modelled cell surface temperatures T_s are reported.

Table 3. The thermal model parameters obtained from the thermal characterization tests for the four tested cell models.

	C_c	R_c	R_{u1}	R_{u2}
	[J/K]	[K/W]	[K/W]	[K/W]
P28A	56.3	0.41	6.02	1.07
P28B	55.7	0.24	5.54	2.49
P30B	70.2	0.10	4.94	0.80
VTC5D	68.6	0.15	5.54	1.90

 doi:10.20944/preprints202405.1399.v1

4. Model Validation

To validate the battery model, four different load profiles have been considered.

The first and the second are taken from common autmotive sector oriented testing profiles, respectively the Beijing Dynamic Stress Test (BJDST) and the Federal Urban Driving Schedule (FUDS) [51]. The third profile is named Non-Dynamic Cycle (NDC) and it accounts for non intensive electrical device loads, like smartphones or low usage systems [10]. The fourth is the High Power Load (HPL) profile, characterized by high magnitude discharge current peaks (up to 10 C) [7].

The BJDST, FUDS and NDC profiles were used to validated the model voltage prediction for the batteries considered, while HPL was also targeting the validation of T_s model prediction.

Experimental data were collected using the testing facility described above, the thermal chamber air temperature equal to 24 °C.

Validation results for BJDST and FUDS profiles are reported in Figures 10 and in 11, while Figures 12 and 13 account for the NDC and the HPL profiles respectively. In Table 4, the Root Mean Square Error (RMSE) for the various profiles tested are reported.

The results show that voltages are predicted with a RMSE lower than 20 mV, while T_s predicition presents a RMSE lower than 0.3 K. It is worth noting how the ECM could be further improved. In particular, the actual Coulomb counting based *SoC* estimation could be enhanced by using an optimization routine (*e.g.*, Kalman filter). In this way, the dependence of the battery capacity on the load could be better accounted: in the actual work, a charge/discharge η equal to 0.9 was considered. Furthermore, an hysteretic behaviour was noted when measuring the OCV, in particular for the Molicel P30B (that presents the higher errors on voltage prediction): this could be considered adding an hysteresis term in V_t prediction as in [10].

Table 4. The RMS for the validation profiles considered for the P28A, P28B, P30B and VTC5D cell.

	BJDST	**FUDS**	**NDC**	**HPL**	
	RMSE, V_t	**RMSE, V_t**	**RMSE, V_t**	**RMSE, V_t**	**RMSE, T_s**
	[mV]	**[mV]**	**[mV]**	**[mV]**	**[°C]**
P28A	4.4	7.3	17.7	15.4	0.21
P28B	5.7	14.7	12.9	16.5	0.30
P30B	13.4	13.5	18.9	17.8	0.20
VTC5D	5.3	8.8	13.6	15.9	0.25

 doi:10.20944/preprints202405.1399.v1

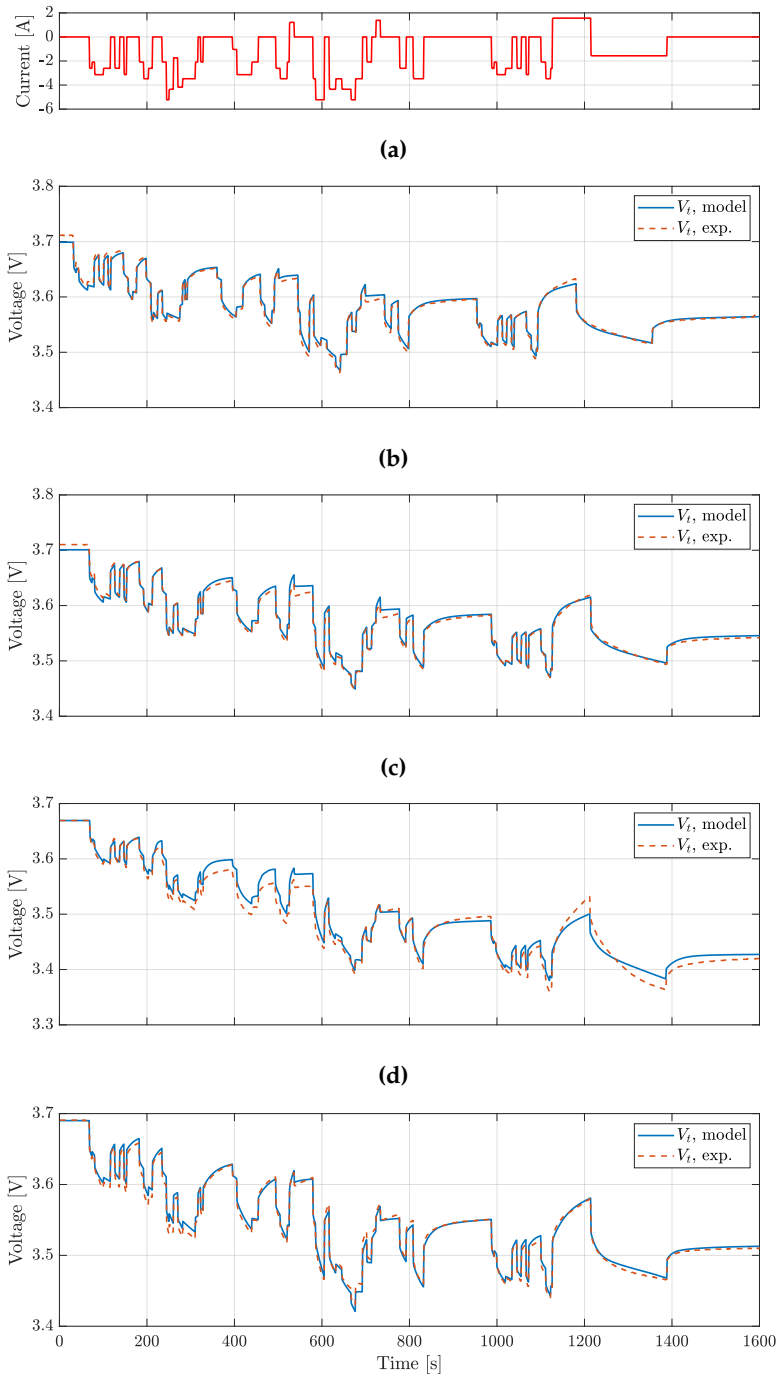

Figure 10. The results of BJDST validation profile: (**a**) show the current profile, (**b**) shows the modelled and experimental V_t for the P28A cell, (**c**) for the P28B cell, (**d**) for the P30B and (**e**) for the VTC5D cell.

 doi:10.20944/preprints202405.1399.v1

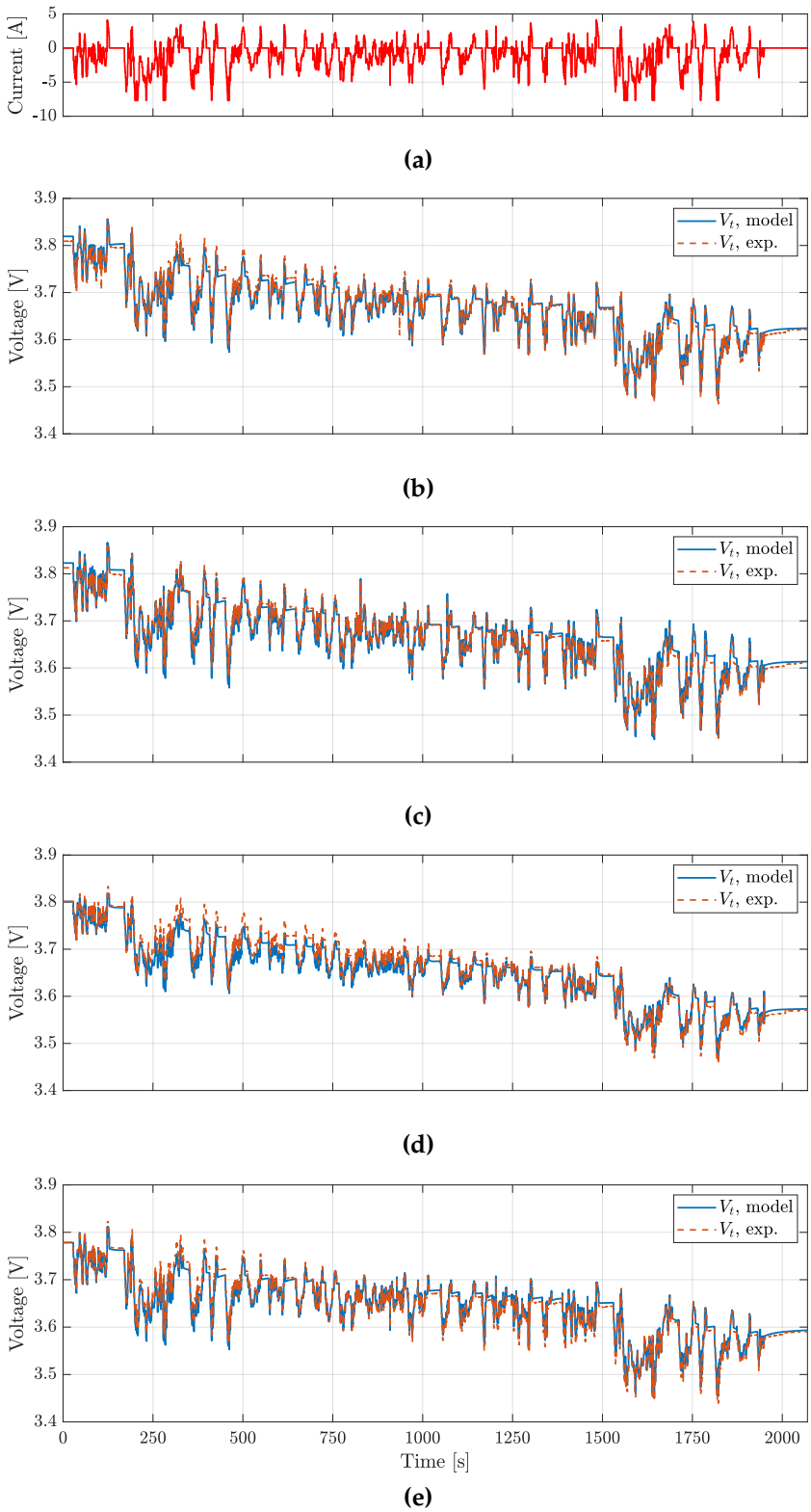

Figure 11. The results of FUDS validation profile: (**a**) show the current profile, (**b**) shows the modelled and experimental V_t for the P28A cell, (**c**) for the P28B cell, (**d**) for the P30B and (**e**) for the VTC5D cell.

Preprints.org (www.preprints.org) | NOT PEER-REVIEWED | Posted: 21 May 2024 doi:10.20944/preprints202405.1399.v1

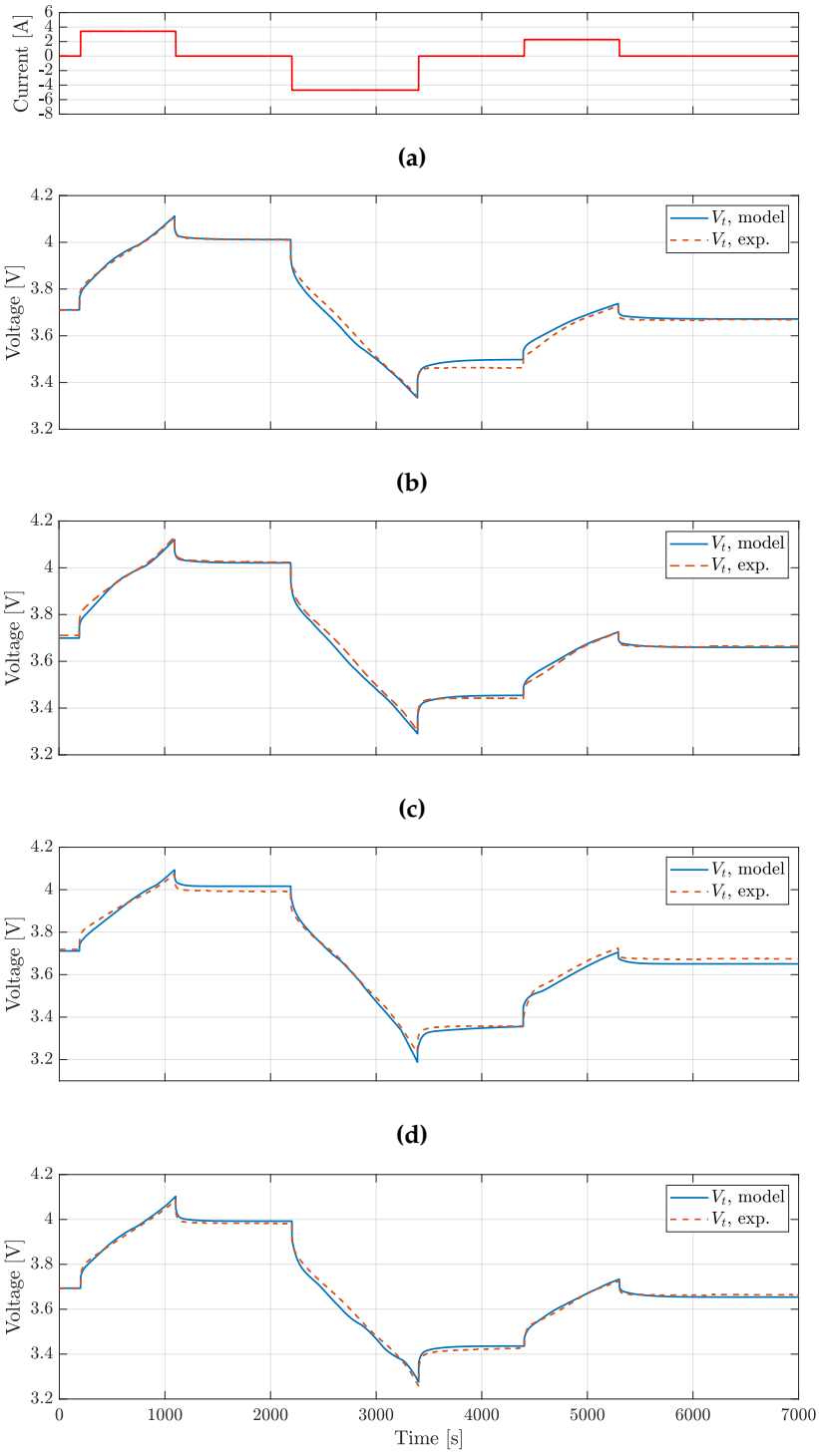

Figure 12. The results of NDC validation profile: (**a**) show the current profile, (**b**) shows the modelled and experimental V_t for the P28A cell, (**c**) for the P28B cell, (**d**) for the P30B and (**e**) for the VTC5D cell.

Preprints.org (www.preprints.org) | NOT PEER-REVIEWED | Posted: 21 May 2024 doi:10.20944/preprints202405.1399.v1

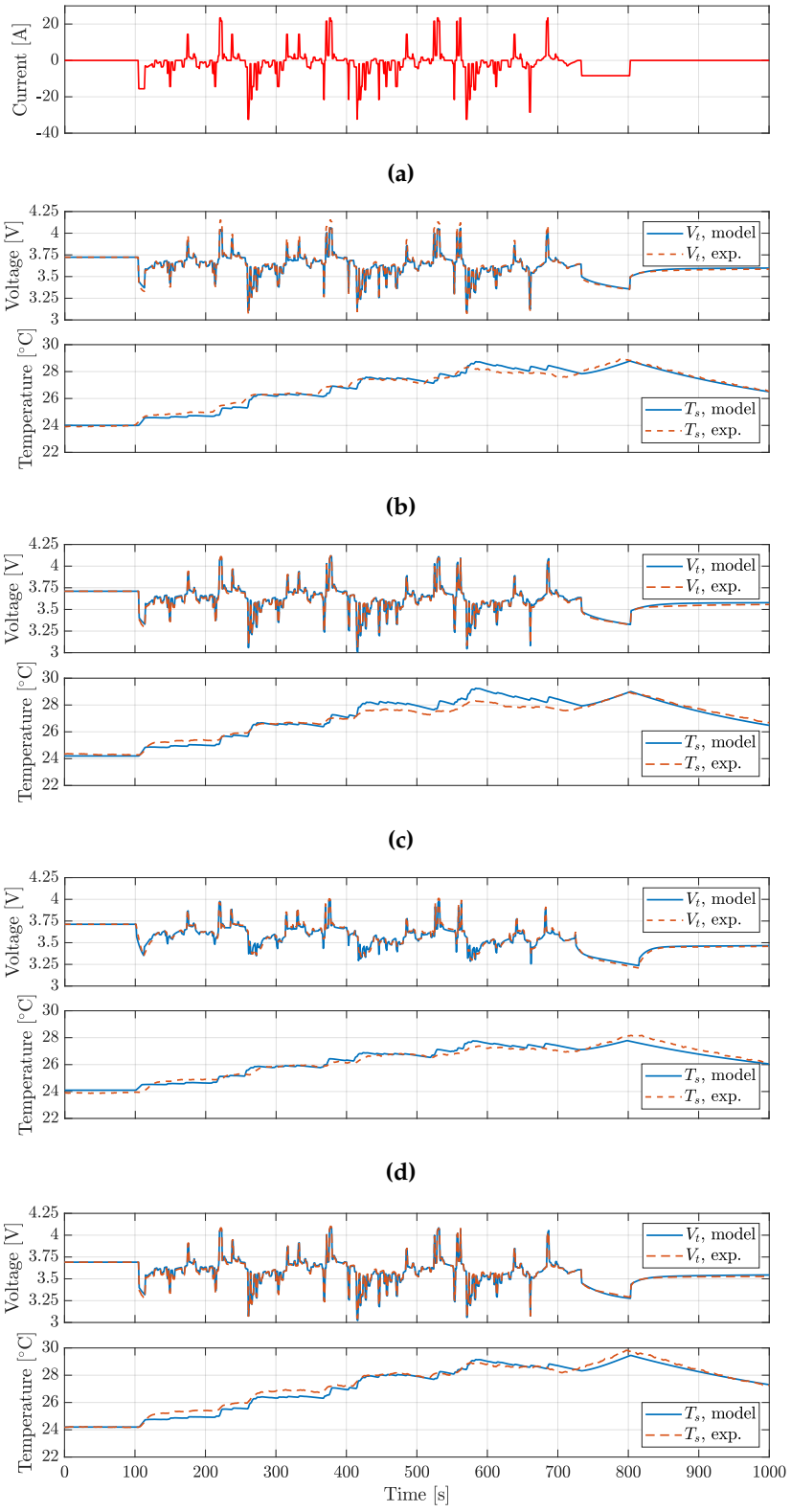

Figure 13. The results of HPL validation profile: (**a**) show the current profile, (**b**) shows the modelled and experimental V_t and T_s for the P28A cell, (**c**) for the P28B cell, (**d**) for the P30B and (**e**) for the VTC5D cell.

 doi:10.20944/preprints202405.1399.v1

5. Conclusions

In this work, a group of four different market available 18650 Li-ion cells consisting of Molicel P28A, P28B and P30B and Sony Murata VTC5D was tested and characterized.

The CC discharge performance were measured for all the cells at operating temperature of 5 °C, 25 °C and 40 °C and C-rate of 0.5 C, 1 C, 3 C and 5 C. Performance spreading was accounted giving the standard deviation over a sample of 3 cells per model.

A second order *RC* ECM model was characterized: first the OCV curves were measured through a pseudo-U_{oc} technique, then the ECM parameters were extrapolated using a Matlab based algorithm from GITT tests at various temperatures and *SoC*.

Furthermore, the entropic contribution was measured using a PAM approach. This resulted in shortening the time needed to measure the temperature derivative of the OCV at various *SoC*, without the need for expensive equipment as calorimeters or complex modelling. Results obtained showed a good agreement with literature for NMC based cells.

Moreover, the thermal behaviour of the cells was described using a thermal lumped parameters model, that has been characterized using only temperatures data.

The coupled model was validated over three dynamic and one non-dynamic load profiles. Battery terminals voltages were predicted with an RMSE lower than 20 mV, while the battery surface temperature prediction RMSE was lower than 0.3 K. Further developments of the ECM model can consider the addition of Kalman filter to predict the battery *SoC* over longer simulations and improving the circuit taking into account voltage hysteresis phenomena.

It is worth noting how overall performance of Molicel P28A, P28B and Sony Murata VTC5D are pretty close: in particular, given the same current load profile, overvoltages are similar, thus giving a similar thermal behaviour. On the contrary, the Molicel P30B, considering its higher nominal capacity results in lower overvoltages and in a lower temperature rise considering the same testing profile.

Author Contributions: Conceptualization, N.Z.; methodology, N.Z.; software, N.Z., B.D., E.D., G.C1.; validation, N.Z. and B.D.; formal analysis, A.T. and M.G.; investigation, N.Z.; resources, B.D. and G.C2.; data curation, N.Z. and B.D.; writing original draft preparation, N.Z.; writing, review and editing, A.L., A.T. and M.G.; visualization, N.Z.; supervision, G.C2., A.L. and M.G.; project administration, M.G.; funding acquisition, A.L. and M.G. All authors have read and agreed to the published version of the manuscript.

Funding: This research received no external funding.

Institutional Review Board Statement: Not applicable.

Informed Consent Statement: Not applicable.

Data Availability Statement: The data presented in this study are available on request from the corresponding author. The data are not publicly available due to confidentiality.

Acknowledgments: This work was supported by FIAMM Energy Technologies, Montecchio Maggiore, Italy.

Conflicts of Interest: The authors declare no conflict of interest.

Sample Availability: Samples of the compounds ... are available from the authors.

 doi:10.20944/preprints202405.1399.v1

Abbreviations

The following abbreviations are used in this manuscript:

ARC	Accelerating Rate Calorimeter
BJDST	Beijing Dynamic Stress Test
BMS	Battery Management System
CC	Constant Current
CPM	Common Potentiometric Method
CV	Constant Voltage
ECM	Equivalent Circuit Model
EIS	Electrothermal Impedance Spectroscopy
FSAE	Formula of the Society of Automotive Engineers
FUDS	Federal Urban Driving Schedule
HPL	High Power Load
NDC	Non Dynamic Cycle
OCV	Open Circuit Voltage
PAM	Positive Adjustment Method
RMSE	Root Mean Square Error
SoC	State Of Charge

Appendix A

Appendix A.1

Here are reported the table containing the ECM parameters for the different cells 386 tested at 5, 25 and 40 °C.

 doi:10.20944/preprints202405.1399.v1

Table A1. The ECM parameters for the P28A cell model.

$T_c = 5°C$										
	Discharge					Charge				
SoC	R_s	R_1	C_1	R_2	C_2	R_s	R_1	C_1	R_2	C_2
	[Ω]	[Ω]	[F]	[Ω]	[F]	[Ω]	[Ω]	[F]	[Ω]	[F]
0.1	0.0271	0.0308	1173	0.0196	21 970	0.0266	0.0433	8526	0.0355	24 350
0.2	0.0263	0.0219	1412	0.0211	33 364	0.0242	0.0662	4058	0.0281	21 050
0.3	0.0264	0.0230	1573	0.0225	42 927	0.0222	0.0570	512	0.0155	20 215
0.4	0.0269	0.0216	1197	0.0154	40 665	0.0218	0.0171	886	0.0268	16 880
0.5	0.0272	0.0178	819	0.0130	33 119	0.0217	0.0132	823	0.0110	20 650
0.6	0.0273	0.0152	646	0.0190	23 145	0.0208	0.0127	941	0.0092	21 596
0.7	0.0283	0.0134	775	0.0325	15 821	0.0227	0.0148	1085	0.0135	31 539
0.8	0.0305	0.0183	959	0.0397	11 399	0.0284	0.0114	1531	0.0140	34 055
0.9	0.0313	0.0215	999	0.0180	24 522	0.0331	0.0059	2139	0.0096	22 909
$T_c = 25°C$										
	Discharge					Charge				
SoC	R_s	R_1	C_1	R_2	C_2	R_s	R_1	C_1	R_2	C_2
	[Ω]	[Ω]	[F]	[Ω]	[F]	[Ω]	[Ω]	[F]	[Ω]	[F]
0.1	0.0191	0.0128	2345	0.0101	21 935	0.0166	0.0098	1141	0.0110	38 210
0.2	0.0170	0.0083	1844	0.0080	19 192	0.0160	0.0092	2314	0.0109	53 291
0.3	0.0165	0.0106	2187	0.0101	29 387	0.0155	0.0069	1735	0.0099	38 424
0.4	0.0170	0.0106	1833	0.0069	36 820	0.0152	0.0068	1847	0.0068	34 442
0.5	0.0173	0.0077	1408	0.0063	30 551	0.0152	0.0093	2521	0.0082	49 947
0.6	0.0174	0.0073	1192	0.0121	35 108	0.0154	0.0084	2256	0.0075	45 617
0.7	0.0173	0.0085	1375	0.0193	24 324	0.0155	0.0073	1505	0.0046	36 110
0.8	0.0179	0.0106	1953	0.0125	19 786	0.0161	0.0110	1623	0.0052	43 433
0.9	0.0184	0.0106	1874	0.0056	90 703	0.0148	0.0144	2441	0.0116	63 415
$T_c = 40°C$										
	Discharge					Charge				
SoC	R_s	R_1	C_1	R_2	C_2	R_s	R_1	C_1	R_2	C_2
	[Ω]	[Ω]	[F]	[Ω]	[F]	[Ω]	[Ω]	[F]	[Ω]	[F]
0.1	0.0141	0.0169	2955	0.0086	162 380	0.0121	0.0088	1084	0.0203	40 517
0.2	0.0132	0.0094	2871	0.0052	184 930	0.0134	0.0076	2574	0.0142	78 985
0.3	0.0135	0.0092	3330	0.0045	178 230	0.0133	0.0044	1921	0.0121	34 480
0.4	0.0137	0.0101	2264	0.0033	133 110	0.0132	0.0035	1918	0.0063	21 319
0.5	0.0132	0.0082	1705	0.0031	90 442	0.0130	0.0046	2800	0.0059	24 030
0.6	0.0130	0.0068	1995	0.0054	63 078	0.0131	0.0040	2360	0.0050	20 253
0.7	0.0130	0.0094	2733	0.0079	48 266	0.0132	0.0033	2042	0.0038	17 394
0.8	0.0142	0.0085	2367	0.0051	55 187	0.0135	0.0046	2425	0.0050	16 172
0.9	0.0138	0.0074	1858	0.0044	104 600	0.0124	0.0063	2394	0.0096	15 963

 doi:10.20944/preprints202405.1399.v1

Table A2. The ECM parameters for the P28B cell model.

$T_c = 5^\circ C$										
	Discharge					Charge				
SoC	R_s	R_1	C_1	R_2	C_2	R_s	R_1	C_1	R_2	C_2
	[Ω]	[Ω]	[F]	[Ω]	[F]	[Ω]	[Ω]	[F]	[Ω]	[F]
0.1	0.0307	0.0269	1037	0.0222	16 531	0.0312	0.0194	706	0.0409	16 162
0.2	0.0273	0.0220	1333	0.0262	31 633	0.0290	0.0168	930	0.0295	15 259
0.3	0.0271	0.0227	1208	0.0227	33 162	0.0264	0.0139	931	0.0114	19 789
0.4	0.0279	0.0197	915	0.0157	25 628	0.0235	0.0135	932	0.0114	19 789
0.5	0.0276	0.0166	657	0.0136	17 738	0.0220	0.0185	921	0.0164	28 506
0.6	0.0207	0.0143	581	0.0197	13 993	0.0206	0.0212	1121	0.0198	34 355
0.7	0.0289	0.0137	744	0.0367	12 739	0.0192	0.0175	1338	0.0114	19 324
0.8	0.0329	0.0214	911	0.0528	9585	0.0179	0.0190	1303	0.0150	17 600
0.9	0.0345	0.0230	817	0.0334	14 201	0.0166	0.0185	1206	0.0160	21 537
$T_c = 25^\circ C$										
	Discharge					Charge				
SoC	R_s	R_1	C_1	R_2	C_2	R_s	R_1	C_1	R_2	C_2
	[Ω]	[Ω]	[F]	[Ω]	[F]	[Ω]	[Ω]	[F]	[Ω]	[F]
0.1	0.0178	0.0190	2365	0.0105	46 810	0.0161	0.0110	1094	0.0203	23 947
0.2	0.0161	0.0102	1757	0.0078	27 662	0.0155	0.0113	2165	0.0185	44 449
0.3	0.0159	0.0106	2445	0.0104	34 794	0.0147	0.0071	1525	0.0123	29 553
0.4	0.0162	0.0112	1950	0.0071	42 074	0.0142	0.0065	1385	0.0077	25 390
0.5	0.0163	0.0082	1328	0.0060	37 689	0.0139	0.0095	1699	0.0084	37 180
0.6	0.0164	0.0083	1039	0.0115	35 216	0.0137	0.0099	1510	0.0085	37 336
0.7	0.0171	0.0073	1779	0.0202	23 936	0.0138	0.0080	1058	0.0052	26 508
0.8	0.0177	0.0135	1339	0.0146	16 296	0.0138	0.0118	1304	0.0061	33 520
0.9	0.0181	0.0114	1615	0.0067	59 597	0.0158	0.0130	2103	0.0120	47 036
$T_c = 40^\circ C$										
	Discharge					Charge				
SoC	R_s	R_1	C_1	R_2	C_2	R_s	R_1	C_1	R_2	C_2
	[Ω]	[Ω]	[F]	[Ω]	[F]	[Ω]	[Ω]	[F]	[Ω]	[F]
0.1	0.0126	0.0161	2360	0.0084	142 620	0.0120	0.0091	1243	0.0143	32 013
0.2	0.0111	0.0095	1792	0.0047	104 860	0.0116	0.0075	2534	0.0092	75 070
0.3	0.0111	0.0086	2315	0.0046	71 871	0.0116	0.0055	2529	0.0112	59 639
0.4	0.0119	0.0076	2389	0.0048	50 264	0.0112	0.0047	2021	0.0060	41 868
0.5	0.0125	0.0052	1959	0.0050	43 107	0.0106	0.0068	2819	0.0047	53 780
0.6	0.125	0.0051	2382	0.0094	43 637	0.0100	0.0080	2985	0.0053	78 268
0.7	0.0127	0.0083	3214	0.0138	38 551	0.0110	0.0062	1864	0.0033	111 810
0.8	0.0130	0.0092	2863	0.0091	85 219	0.0114	0.0084	2512	0.0046	136 800
0.9	0.0132	0.0071	2231	0.0056	93 891	0.0116	0.0116	2404	0.0073	74 297

 doi:10.20944/preprints202405.1399.v1

Table A3. The ECM parameters for the P30B cell model.

$T_c = 5°C$										
	Discharge					Charge				
SoC	R_s	R_1	C_1	R_2	C_2	R_s	R_1	C_1	R_2	C_2
	[Ω]	[Ω]	[F]	[Ω]	[F]	[Ω]	[Ω]	[F]	[Ω]	[F]
0.1	0.0238	0.0311	1356	0.0406	26 412	0.0228	0.0795	4076	0.0190	50 626
0.2	0.0189	0.0218	1160	0.0231	26 096	0.0207	0.0606	4832	0.0319	60 550
0.3	0.0176	0.0211	1146	0.0274	24 765	0.0174	0.0179	1907	0.0353	57 155
0.4	0.0175	0.0211	1011	0.0295	23 330	0.0142	0.0116	1858	0.0184	29 798
0.5	0.0177	0.0188	824	0.0202	15 980	0.0140	0.0134	1026	0.0110	19 511
0.6	0.0180	0.0135	652	0.0200	10 938	0.0137	0.0158	831	0.0128	28 351
0.7	0.0188	0.0147	742	0.0373	10 167	0.0135	0.0203	965	0.0170	38 968
0.8	0.0213	0.0236	1197	0.0512	16 595	0.0137	0.0173	938	0.0089	34 889
0.9	0.0224	0.0244	1100	0.0202	27 749	0.0145	0.0280	1012	0.0135	47 824
$T_c = 25°C$										
	Discharge					Charge				
SoC	R_s	R_1	C_1	R_2	C_2	R_s	R_1	C_1	R_2	C_2
	[Ω]	[Ω]	[F]	[Ω]	[F]	[Ω]	[Ω]	[F]	[Ω]	[F]
0.1	0.0170	0.0394	1760	0.0255	49 984	0.0114	0.0345	2178	0.0144	62 725
0.2	0.0118	0.0179	1731	0.0115	64 108	0.0106	0.0164	1909	0.0338	48 519
0.3	0.0110	0.0130	1302	0.0083	43 164	0.0096	0.0064	1763	0.0209	23 110
0.4	0.0105	0.0110	1239	0.0082	29 060	0.0094	0.0041	1100	0.0106	11 786
0.5	0.0116	0.0108	1862	0.0090	19 562	0.0094	0.0046	1170	0.0078	11 054
0.6	0.0119	0.0078	1297	0.0076	16 602	0.0093	0.0068	1062	0.0101	16 393
0.7	0.0120	0.0086	1273	0.0138	26 587	0.0095	0.0060	1109	0.0087	14 093
0.8	0.0127	0.0128	2017	0.0168	21 666	0.0096	0.0054	1227	0.0075	7982
0.9	0.0127	0.0125	1652	0.0069	95 862	0.0103	0.0088	1371	0.0132	10 814
$T_c = 40°C$										
	Discharge					Charge				
SoC	R_s	R_1	C_1	R_2	C_2	R_s	R_1	C_1	R_2	C_2
	[Ω]	[Ω]	[F]	[Ω]	[F]	[Ω]	[Ω]	[F]	[Ω]	[F]
0.1	0.0110	0.0274	6336	0.0309	57 321	0.0090	0.0160	1332	0.0651	14 153
0.2	0.0093	0.0131	3732	0.0141	105 080	0.0081	0.0077	1708	0.0662	14 516
0.3	0.0087	0.0103	2516	0.0095	124 580	0.0076	0.0037	1253	0.0245	26 619
0.4	0.0080	0.0083	1943	0.0064	130 980	0.0076	0.0045	900	0.0125	39 521
0.5	0.0084	0.0095	2198	0.0043	90 444	0.0076	0.0061	1006	0.0115	58 670
0.6	0.0092	0.0068	2204	0.0066	75 590	0.0077	0.0070	1493	0.0081	37 061
0.7	0.0093	0.0070	2610	0.0066	78 856	0.0078	0.0054	1540	0.0081	37 061
0.8	0.0095	0.0102	3046	0.0073	75 567	0.0080	0.0045	1549	0.0053	36 016
0.9	0.0095	0.0077	2187	0.0054	129 950	0.0083	0.0083	2227	0.0081	50 669

 doi:10.20944/preprints202405.1399.v1

Table A4. The ECM parameters for the VTC5D cell model.

$T_c = 5^\circ C$										
	Discharge					Charge				
SoC	R_s	R_1	C_1	R_2	C_2	R_s	R_1	C_1	R_2	C_2
	[Ω]	[Ω]	[F]	[Ω]	[F]	[Ω]	[Ω]	[F]	[Ω]	[F]
0.1	0.0265	0.0330	1125	0.0271	11 198	0.0291	0.0219	658	0.0450	8029
0.2	0.0249	0.0188	1367	0.0154	15 964	0.0266	0.0067	768	0.0324	3196
0.3	0.0238	0.0215	1650	0.0197	25 405	0.0232	0.0073	804	0.0168	5071
0.4	0.0235	0.0243	1814	0.0218	31 775	0.0216	0.0066	1080	0.0144	5541
0.5	0.0238	0.0206	1440	0.0149	30 667	0.0216	0.0096	962	0.0211	6901
0.6	0.0243	0.0173	1222	0.0151	30 607	0.0218	0.0117	647	0.0214	7393
0.7	0.0254	0.0159	1552	0.0287	26 171	0.0227	0.0121	818	0.0128	6113
0.8	0.0273	0.0259	1767	0.0387	20 423	0.0264	0.0160	1208	0.0145	8581
0.9	0.0294	0.0259	1251	0.0154	34 463	0.0402	0.0245	2300	0.0450	17 704
$T_c = 25^\circ C$										
	Discharge					Charge				
SoC	R_s	R_1	C_1	R_2	C_2	R_s	R_1	C_1	R_2	C_2
	[Ω]	[Ω]	[F]	[Ω]	[F]	[Ω]	[Ω]	[F]	[Ω]	[F]
0.1	0.0227	0.0165	2772	0.0123	15 823	0.0163	0.0358	2089	0.0175	62 603
0.2	0.0176	0.0089	1832	0.0066	19 355	0.0154	0.0133	2257	0.0234	51 085
0.3	0.0158	0.0105	1741	0.0078	17 670	0.0147	0.0106	1727	0.0230	24 814
0.4	0.0151	0.0123	1760	0.0092	17 286	0.0144	0.0070	1581	0.0118	15 220
0.5	0.0156	0.0086	1208	0.0097	13 320	0.0144	0.0082	1632	0.0103	16 589
0.6	0.0160	0.0079	1198	0.0186	17 363	0.0146	0.0084	1337	0.0094	16 235
0.7	0.0160	0.0114	1898	0.0259	24 139	0.0150	0.0080	1328	0.0057	14 737
0.8	0.0167	0.0146	2295	0.0157	18 389	0.0158	0.0115	1324	0.0058	21 896
0.9	0.0174	0.0127	1965	0.0061	37 337	0.0137	0.0197	1617	0.0121	41 477
$T_c = 40^\circ C$										
	Discharge					Charge				
SoC	R_s	R_1	C_1	R_2	C_2	R_s	R_1	C_1	R_2	C_2
	[Ω]	[Ω]	[F]	[Ω]	[F]	[Ω]	[Ω]	[F]	[Ω]	[F]
0.1	0.0150	0.0184	2727	0.0086	80 205	0.0116	0.0193	1153	0.0372	18 047
0.2	0.0138	0.0093	2013	0.0043	44 757	0.0117	0.0099	1311	0.0184	40 515
0.3	0.0127	0.0083	1614	0.0041	30 351	0.0120	0.0078	1806	0.0160	55 242
0.4	0.0124	0.0089	1788	0.0060	20 576	0.0123	0.0069	1619	0.0083	45 626
0.5	0.0133	0.0063	1975	0.0066	16 017	0.0122	0.0084	1929	0.0078	38 101
0.6	0.0133	0.0057	2361	0.0062	21 600	0.0123	0.0068	1826	0.0065	32 643
0.7	0.0134	0.0090	3291	0.0090	31 691	0.0127	0.0060	1701	0.0040	34 223
0.8	0.0137	0.0096	2348	0.0056	21 288	0.0131	0.0083	1671	0.0044	39 989
0.9	0.0141	0.0058	2081	0.0039	10 820	0.0116	0.0142	1904	0.0087	61 896

References

1. Bashir, T.; Ismail, S.A.; Song, Y.; Irfan, R.M.; Yang, S.; Zhou, S.; Zhaou, J.; Gao, L. A review of the energy storage aspects of chemical elements for lithium-ion based batteries. *Energy Materials* **2021**, *1*, 100019. doi:http://dx.doi.org/10.20517/energymater.2021.20.
2. Kumar, R.; Goel, V. A study on thermal management system of lithium-ion batteries for electrical vehicles: A critical review. *Journal of Energy Storage* **2023**, *71*, 108025. doi:https://doi.org/10.1016/j.est.2023.108025.
3. Abdalla, A.M.; Abdullah, M.F.; Dawood, M.K.; Wei, B.; Subramanian, Y.; Azad, A.T.; Nourin, S.; Afroze, S.; Taweekun, J.; Azad, A.K. Innovative lithium-ion battery recycling: Sustainable process for recovery of critical materials from lithium-ion batteries. *Journal of Energy Storage* **2023**, *67*, 107551. doi:https://doi.org/10.1016/j.est.2023.107551.

4. Jaguemont, J.; Boulon, L.; Dubé, Y. A comprehensive review of lithium-ion batteries used in hybrid and electric vehicles at cold temperatures. *Applied Energy* **2016**, *164*, 99–114. doi:https://doi.org/10.1016/j.apenergy.2015.11.034.
5. Adaikkappan, M.; Sathiyamoorthy, N. Modeling, state of charge estimation, and charging of lithium-ion battery in electric vehicle: A review. *International Journal of Energy Research* **2022**, *46*, 2141–2165, [https://onlinelibrary.wiley.com/doi/pdf/10.1002/er.7339]. doi:https://doi.org/10.1002/er.7339.
6. Barcellona, S.; Piegari, L. Lithium Ion Battery Models and Parameter Identification Techniques. *Energies* **2017**, *10*. doi:10.3390/en10122007.
7. Ekström, H.; Fridholm, B.; Lindbergh, G. Comparison of lumped diffusion models for voltage prediction of a lithium-ion battery cell during dynamic loads. *Journal of Power Sources* **2018**, *402*, 296–300. doi:https://doi.org/10.1016/j.jpowsour.2018.09.020.
8. Jackey, R.; Saginaw, M.; Sanghvi, P.; Gazzarri, J.; Huria, T.; Ceraolo, M. Battery Model Parameter Estimation Using a Layered Technique: An Example Using a Lithium Iron Phosphate Cell. *SAE Technical Paper* **2013**, *1547*. doi:https://doi.org/10.4271/2013-01-1547.
9. Akbarzadeh, M.; Kalogiannis, T.; Jaguemont, J.; He, J.; Jin, L.; Berecibar, M.; Van Mierlo, J. Thermal modeling of a high-energy prismatic lithium-ion battery cell and module based on a new thermal characterization methodology. *Journal of Energy Storage* **2020**, *32*, 101707. doi:https://doi.org/10.1016/j.est.2020.101707.
10. Tran, M.K.; DaCosta, A.; Mevawalla, A.; Panchal, S.; Fowler, M. Comparative Study of Equivalent Circuit Models Performance in Four Common Lithium-Ion Batteries: LFP, NMC, LMO, NCA. *Batteries* **2021**, *7*. doi:10.3390/batteries7030051.
11. Hua, X.; Zhang, C.; Offer, G. Finding a better fit for lithium ion batteries: A simple, novel, load dependent, modified equivalent circuit model and parameterization method. *Journal of Power Sources* **2021**, *484*, 229117. doi:https://doi.org/10.1016/j.jpowsour.2020.229117.
12. Lin, X.; Perez, H.E.; Mohan, S.; Siegel, J.B.; Stefanopoulou, A.G.; Ding, Y.; Castanier, M.P. A lumped-parameter electro-thermal model for cylindrical batteries. *Journal of Power Sources* **2014**, *257*, 1–11. doi:https://doi.org/10.1016/j.jpowsour.2014.01.097.
13. Madani, S.S.; Schaltz, E.; Knudsen Kær, S. Review of Parameter Determination for Thermal Modeling of Lithium Ion Batteries. *Batteries* **2018**, *4*. doi:10.3390/batteries4020020.
14. Chin, C.; Gao, Z.; Zhang, C. Comprehensive electro-thermal model of 26650 lithium battery for discharge cycle under parametric and temperature variations. *Journal of Energy Storage* **2020**, *28*, 101222. doi:https://doi.org/10.1016/j.est.2020.101222.
15. Forgez, C.; Vinh Do, D.; Friedrich, G.; Morcrette, M.; Delacourt, C. Thermal modeling of a cylindrical LiFePO4/graphite lithium-ion battery. *Journal of Power Sources* **2010**, *195*, 2961–2968. doi:https://doi.org/10.1016/j.jpowsour.2009.10.105.
16. Asus, Z.; Aglzim, E.H.; Chrenko, D.; Daud, Z.H.C.; Le Moyne, L. Dynamic Modeling and Driving Cycle Prediction for a Racing Series Hybrid Car. *IEEE Journal of Emerging and Selected Topics in Power Electronics* **2014**, *2*, 541–551. doi:10.1109/JESTPE.2014.2307079.
17. Mattarelli, E.; Rinaldini, C.A.; Scrignoli, F.; Mangeruga, V. Development of a Hybrid Power Unit for Formula SAE Application: ICE CFD-1D Optimization and Vehicle Lap Simulation. 14th International Conference on Engines & Vehicles. SAE International, 2019. doi:https://doi.org/10.4271/2019-24-0200.
18. *Conceptual Design of a Formula Hybrid Powertrain System Utilizing Functionality-Based Modeling Tools*, Vol. Volume 5: 22nd International Conference on Design Theory and Methodology; Special Conference on Mechanical Vibration and Noise, *International Design Engineering Technical Conferences and Computers and Information in Engineering Conference*, 2010. doi:10.1115/DETC2010-28836.
19. Muenzel, V.; Hollenkamp, A.F.; Bhatt, A.I.; de Hoog, J.; Brazil, M.; Thomas, D.A.; Mareels, I. A Comparative Testing Study of Commercial 18650-Format Lithium-Ion Battery Cells. *Journal of The Electrochemical Society* **2015**, *162*, A1592. doi:10.1149/2.0721508jes.
20. Braco, E.; San Martín, I.; Berrueta, A.; Sanchis, P.; Ursúa, A. Experimental assessment of cycling ageing of lithium-ion second-life batteries from electric vehicles. *Journal of Energy Storage* **2020**, *32*, 101695. doi:https://doi.org/10.1016/j.est.2020.101695.

21. Waldmann, T.; Scurtu, R.G.; Richter, K.; Wohlfahrt-Mehrens, M. 18650 vs. 21700 Li-ion cells – A direct comparison of electrochemical, thermal, and geometrical properties. *Journal of Power Sources* **2020**, *472*, 228614. doi:https://doi.org/10.1016/j.jpowsour.2020.228614.
22. Mulpuri, S.K.; Sah, B.; Kumar, P. Protocol for conducting advanced cyclic tests in lithium-ion batteries to estimate capacity fade. *STAR Protocols* **2024**, *5*, 102938. doi:https://doi.org/10.1016/j.xpro.2024.102938.
23. Baumhöfer, T.; Brühl, M.; Rothgang, S.; Sauer, D.U. Production caused variation in capacity aging trend and correlation to initial cell performance. *Journal of Power Sources* **2014**, *247*, 332–338. doi:https://doi.org/10.1016/j.jpowsour.2013.08.108.
24. Soto, A.; Berrueta, A.; Sanchis, P.; Ursúa, A. Analysis of the main battery characterization techniques and experimental comparison of commercial 18650 Li-ion cells. 2019 IEEE International Conference on Environment and Electrical Engineering and 2019 IEEE Industrial and Commercial Power Systems Europe (EEEIC / I & CPS Europe), 2019, pp. 1–6. doi:10.1109/EEEIC.2019.8783862.
25. Ren, Z.; Du, C.; Wu, Z.; Shao, J.; Deng, W. A comparative study of the influence of different open circuit voltage tests on model-based state of charge estimation for lithium-ion batteries. *International Journal of Energy Research* **2021**, *45*, 13692–13711, [https://onlinelibrary.wiley.com/doi/pdf/10.1002/er.6700]. doi:https://doi.org/10.1002/er.6700.
26. Pillai, P.; Sundaresan, S.; Kumar, P.; Pattipati, K.R.; Balasingam, B. Open-Circuit Voltage Models for Battery Management Systems: A Review. *Energies* **2022**, *15*. doi:10.3390/en15186803.
27. Pillai, P.; Nguyen, J.; Balasingam, B. Performance Analysis of Empirical Open-Circuit Voltage Modeling in Lithium-ion Batteries, Part-2: Data Collection Procedure. *IEEE Transactions on Transportation Electrification* **2024**, pp. 1–1. doi:10.1109/TTE.2024.3386910.
28. Baronti, F.; Zamboni, W.; Roncella, R.; Saletti, R.; Spagnuolo, G. Open-circuit voltage measurement of Lithium-Iron-Phosphate batteries. 2015 IEEE International Instrumentation and Measurement Technology Conference (I2MTC) Proceedings, 2015, pp. 1711–1716. doi:10.1109/I2MTC.2015.7151538.
29. Pan, H.; Lü, Z.; Lin, W.; Li, J.; Chen, L. State of charge estimation of lithium-ion batteries using a grey extended Kalman filter and a novel open-circuit voltage model. *Energy* **2017**, *138*, 764–775. doi:https://doi.org/10.1016/j.energy.2017.07.099.
30. Samieian, M.A.; Hales, A.; Patel, Y. A Novel Experimental Technique for Use in Fast Parameterisation of Equivalent Circuit Models for Lithium-Ion Batteries. *Batteries* **2022**, *8*. doi:10.3390/batteries8090125.
31. Zhang, X.F.; Zhao, Y.; Patel, Y.; Zhang, T.; Liu, W.M.; Chen, M.; Offer, G.J.; Yan, Y. Potentiometric measurement of entropy change for lithium batteries. *Phys. Chem. Chem. Phys.* **2017**, *19*, 9833–9842. doi:10.1039/C6CP08505A.
32. Eddahech, A.; Briat, O.; Vinassa, J.M. Thermal characterization of a high-power lithium-ion battery: Potentiometric and calorimetric measurement of entropy changes. *Energy* **2013**, *61*, 432–439. doi:https://doi.org/10.1016/j.energy.2013.09.028.
33. Geng, Z.; Groot, J.; Thiringer, T. A Time- and Cost-Effective Method for Entropic Coefficient Determination of a Large Commercial Battery Cell. *IEEE Transactions on Transportation Electrification* **2020**, *6*, 257–266.
34. Xiao, M.; Choe, S.Y. Theoretical and experimental analysis of heat generations of a pouch type LiMn2O4/carbon high power Li-polymer battery. *Journal of Power Sources* **2013**, *241*, 46–55. doi:https://doi.org/10.1016/j.jpowsour.2013.04.062.
35. Damay, N.; Forgez, C.; Bichat, M.P.; Friedrich, G. A method for the fast estimation of a battery entropy-variation high-resolution curve – Application on a commercial LiFePO4/graphite cell. *Journal of Power Sources* **2016**, *332*, 149–153. doi:https://doi.org/10.1016/j.jpowsour.2016.09.083.
36. Schmidt, J.P.; Weber, A.; Ivers-Tiffée, E. A novel and precise measuring method for the entropy of lithium-ion cells: ΔS via electrothermal impedance spectroscopy. *Electrochimica Acta* **2014**, *137*, 311–319. doi:https://doi.org/10.1016/j.electacta.2014.05.153.
37. Hudak, N.S.; Davis, L.E.; Nagasubramanian, G. Cycling-Induced Changes in the Entropy Profiles of Lithium Cobalt Oxide Electrodes. *Journal of The Electrochemical Society* **2014**, *162*, A315. doi:10.1149/2.0071503jes.
38. Lin, Z.; Wu, D.; Du, C.; Ren, Z. An improved potentiometric method for the measurement of entropy coefficient of lithium-ion battery based on positive adjustment. *Energy Reports* **2022**, *8*, 54–63. 2022 The 5th International Conference on Renewable Energy and Environment Engineering, doi:https://doi.org/10.1016/j.egyr.2022.10.109.

 doi:10.20944/preprints202405.1399.v1

39. Zhao, W.; Rohde, M.; Mohsin, I.U.; Ziebert, C.; Seifert, H.J. Heat Generation in NMC622 Coin Cells during Electrochemical Cycling: Separation of Reversible and Irreversible Heat Effects. *Batteries* **2020**, *6*. doi:10.3390/batteries6040055.
40. Vertiz, G.; Oyarbide, M.; Macicior, H.; Miguel, O.; Cantero, I.; Fernandez de Arroiabe, P.; Ulacia, I. Thermal characterization of large size lithium-ion pouch cell based on 1d electro-thermal model. *Journal of Power Sources* **2014**, *272*, 476–484. doi:https://doi.org/10.1016/j.jpowsour.2014.08.092.
41. Sheng, L.; Su, L.; Zhang, H. Experimental determination on thermal parameters of prismatic lithium ion battery cells. *International Journal of Heat and Mass Transfer* **2019**, *139*, 231–239. doi:https://doi.org/10.1016/j.ijheatmasstransfer.2019.04.143.
42. Cao, R.; Zhang, X.; Yang, H.; Wang, C. Experimental study on heat generation characteristics of lithium-ion batteries using a forced convection calorimetry method. *Applied Thermal Engineering* **2023**, *219*, 119559. doi:https://doi.org/10.1016/j.applthermaleng.2022.119559.
43. Tahir, M.W.; Merten, C. Multi-scale thermal modeling, experimental validation, and thermal characterization of a high-power lithium-ion cell for automobile application. *Energy Conversion and Management* **2022**, *258*, 115490. doi:https://doi.org/10.1016/j.enconman.2022.115490.
44. E, J.; Yue, M.; Chen, J.; Zhu, H.; Deng, Y.; Zhu, Y.; Zhang, F.; Wen, M.; Zhang, B.; Kang, S. Effects of the different air cooling strategies on cooling performance of a lithium-ion battery module with baffle. *Applied Thermal Engineering* **2018**, *144*, 231–241. doi:https://doi.org/10.1016/j.applthermaleng.2018.08.064.
45. Nie, P.; Zhang, S.W.; Ran, A.; Yang, C.; Chen, S.; Li, Z.; Zhang, X.; Deng, W.; Liu, T.; Kang, F.; Wei, G. Full-cycle electrochemical-thermal coupling analysis for commercial lithium-ion batteries. *Applied Thermal Engineering* **2021**, *184*, 116258. doi:https://doi.org/10.1016/j.applthermaleng.2020.116258.
46. Al-Zareer, M.; Ebbs-Picken, T.; Michalak, A.; Escobar, C.; Da Silva, C.M.; Davis, T.; Osio, I.; Amon, C.H. Heat generation rates and anisotropic thermophysical properties of cylindrical lithium-ion battery cells with different terminal mounting configurations. *Applied Thermal Engineering* **2023**, *223*, 119990. doi:https://doi.org/10.1016/j.applthermaleng.2023.119990.
47. Samad, N.A.; Wang, B.; Siegel, J.B.; Stefanopoulou, A.G. Parameterization of Battery Electrothermal Models Coupled With Finite Element Flow Models for Cooling. *Journal of Dynamic Systems, Measurement, and Control* **2017**, *139*, 071003, [https://asmedigitalcollection.asme.org/dynamicsystems/article-pdf/139/7/071003/6124140/ds_139_07_071003.pdf]. doi:10.1115/1.4035742.
48. Lin, X.; Perez, H.E.; Siegel, J.B.; Stefanopoulou, A.G.; Li, Y.; Anderson, R.D.; Ding, Y.; Castanier, M.P. Online Parameterization of Lumped Thermal Dynamics in Cylindrical Lithium Ion Batteries for Core Temperature Estimation and Health Monitoring. *IEEE Transactions on Control Systems Technology* **2013**, *21*, 1745–1755. doi:10.1109/TCST.2012.2217143.
49. Farag, M.; Sweity, H.; Fleckenstein, M.; Habibi, S. Combined electrochemical, heat generation, and thermal model for large prismatic lithium-ion batteries in real-time applications. *Journal of Power Sources* **2017**, *360*, 618–633. doi:https://doi.org/10.1016/j.jpowsour.2017.06.031.
50. Bryden, T.S.; Dimitrov, B.; Hilton, G.; Ponce de León, C.; Bugryniec, P.; Brown, S.; Cumming, D.; Cruden, A. Methodology to determine the heat capacity of lithium-ion cells. *Journal of Power Sources* **2018**, *395*, 369–378. doi:https://doi.org/10.1016/j.jpowsour.2018.05.084.
51. Battery Data: Center for Advanced Life Cycle Engingeering (CALCE), University of Maryland, 2016. https://calce.umd.edu/battery-data#Storage [Accessed: February 1st, 2024].